Efficient loading of silver nanoparticles on graphene oxide and its antibacterial properties

NANO EXPRESS

PAPER

Efficient loading of silver nanoparticles on graphene oxide and its antibacterial properties

Hui Wang[1], **Yalei Zhang**[2], **Xiaobing Xu**[1], **Feiyao Yang**[1], **Ke Li**[1], **Di Wei**[1,3] and **Zhongfan Liu**[1,2]

[1] Beijing Graphene Institute, Beijing 100094, People's Republic of China
[2] Center for Nanochemistry, Beijing Science and Engineering Center for Nanocarbons, Beijing National Laboratory for Molecular Sciences, College of Chemistry and Molecular Engineering, Peking University, Beijing 100871, People's Republic of China
[3] Authors to whom any correspondence should be addressed.

E-mail: weidi@bgi-graphene.com **and** zfliu@pku.edu.cn

Keywords: silver nanoparticles, graphene oxide, reduced graphene oxide, antibacterial composite

Supplementary material for this article is available online

OPEN ACCESS

RECEIVED
4 March 2020

REVISED
4 May 2020

ACCEPTED FOR PUBLICATION
21 May 2020

PUBLISHED
4 June 2020

Abstract

Graphene oxide contains polyaromatic structure and a variety of oxygen functional groups, which can form π-type metal ion-aromatic or metal ion-oxygen interaction with transition metals, thus it is a promising dispersant and carrier for silver nanoparticles (AgNPs). Herein, silver nanoparticles/reduced graphene oxide (AgNPs/rGO) was fabricated with scalable synthesis method without additional dispersing agent. The mass percent of AgNPs loading on rGO could be adjusted according to the requirement of applications from 1 $\sim$ 67% of the total weight of AgNPs/rGO with the sizes of AgNPs 10 $\sim$ 30 nm. AgNPs/rGO exhibited excellent antibacterial activity towards both gram-positive *S. aureus* and gram-negative *E. coli*. In addition, AgNPs/rGO could be easily dispersed in liquid silicone rubber, and when the rubber solidified and formed a three-dimensional structure, AgNPs/rGO-silicone rubber has both effective antibacterial property and very low effusion of AgNPs. This composite has potential to be used as a material of bacteriostasis bottles and wound dressings.

1. Introduction

Silver nanoparticles (AgNPs) have played an important role as an excellent bactericide for its advantages of outstanding, broad and durable antibacterial activity [1]. It has been found that the biological activity is related to silver particle size, the smaller the particle size, the more efficient the antibacterial activity [1, 2]. However, with decreasing of silver particle sizes, the surface energy increases and the particles tend to aggregate, thus support materials or surfactants are usually used to maintain the stability.

The traditional carriers of AgNPs are inorganic carriers and organic polymers. The inorganic materials include carbon materials [3, 4], silicon oxide [5, 6], and metallic oxides [7], etc, and AgNPs are attached to the carriers mainly through ion exchange or physical adsorption. The organic polymers are usually polyvinyl alcohol [8], chitosan [9] and cellulose [10, 11], etc, and the interactions between the AgNPs and the carriers are usually charge transfer, electrostatic interaction and hydrogen bond. For conventional carriers, the mass percent of AgNPs loaded is usually between 1% $\sim$ 20% [4, 5, 7, 11, 12], and the low AgNPs loading results in reduced antibacterial property. Further, the effusion of AgNPs in solutions augments when the load of AgNPs increases [3, 10–12], which decreases the durability, as well as increases the safety hazard when AgNPs composites are used as an antibacterial active component of food packaging, tableware and wound dressing etc.

Graphene oxide (GO) is a two-dimensional material with a variety of oxygen functional groups [13] and large surface areas [14], and can be used as an excellent carrier for metal nanoparticles [15–20]. Xu *et al* [21] prepared AgNPs/rGO nanocomposite by using rGO as a carrier and reducing agent and poly(sodium 4-styrenesulfonate) (PSS) as a dispersant, and found that AgNPs/rGO displayed significantly better antibacterial property than that of the pure AgNPs. Mohamed and coworkers [22] synthesized AgNPs/rGO nanocomposite in a two-step method: the first was to reduce AgNPs on GO sheets, and remove the excess of silver ions in

suspension; the second was to deoxidize GO by using potamogeton pectinatus (Po) plant extract to prepare AgNPs/rGO nanocomposite. Ashkarran *et al* [23] fabricated different sizes and shapes of AgNPs, and decorated them on amine functionalized rGO sheets, and then investigated their antibacterial properties.

So far, although there are some reports on the fabrication of AgNPs/rGO, few synthetic methods are fully utilized the molecular structure of GO to prepare AgNPs/rGO composite. GO contains polyaromatic structure and a variety of oxygen functional groups as hydroxyl, carbonyl, and carboxyl in alkaline condition. The carboxyl anion may not only absorb silver ions by electrostatic interaction, but also make the GO sheets further apart by charge repulsion, which allows the silver ions to enter and attach to the nanosheets of GO by π-type silver ion-aromatic [24–26], silver ion-oxygen [27] interaction. Thus GO might be an excellent dispersant for silver ions. What's more, when GO and silver ions are reduced, the layer structure of rGO and the electron transfer between AgNPs and aromatic rings of rGO may restrict the migration of AgNPs [16], which can prolong the antibacterial durability of the AgNPs/rGO composite and reduce the safety hazard when AgNPs/rGO is used as an antibacterial activity component of food packaging, tableware and wound dressing, etc.

In the present work, we took full advantage of the structural characteristics of GO and fabricated AgNPs/rGO by using GO as the dispersant of silver ions and rGO as the carrier of AgNPs. This preparation method might reduce the cost of AgNPs/rGO and was feasible for large-scale production. It was observed that AgNPs/rGO exhibited excellent antibacterial activity towards both gram-positive *Staphylococcus aureus* (*S. aureus*) and gram-negative *Escherichia coli* (*E. coli*). In addition, rGO molecules contains polar groups of hydroxyl and carboxyl and non-polar groups of aromatic rings and may interact with polymer molecules, thus AgNPs/rGO tends to disperse evenly in polymers. For instance, a stable antibacterial composite was prepared by dispersing AgNPs/rGO in liquid silica rubber (LSR), and when the LSR solidified and formed a three-dimensional structure, AgNPs/rGO-silicon rubber (AgNPs/rGO-SR) has both effective antibacterial property and low effusion of AgNPs. This composite has potential to be used as a material of bacteriostasis bottles.

2. Methods

2.1. Materials

Silver nitrate ($AgNO_3$), sodium borohydride ($NaBH_4$) and potassium iodide (KI) were purchased from Aladdin, and sodium hydroxide (NaOH) and ammonium hydroxide ($NH_3.H_2O$) were obtained from Beijing Chemical Company, and all the reagents are analytically pure. GO powder, 1–5 layers, with sheets diameter of 1–5 μm, and thickness of 1.0–1.8 nm was bought from Suzhou Carbon Rich Graphene Company. The Gram-negative bacteria (*E. coli*), and Gram-positive bacteria (*S. aureus*), donated by Prof. Luhua Lai from Peking University, China, were purchased from China General Microbiological Culture Collection Center. The optical density (OD) values of the bacterial suspensions were regulated on a Jasco V-550 spectrometer at 600 nm.

2.2. Characterization

The particle size distribution of GO was evaluated by particle size analyzer (Microtrac Inc., America). The morphology and microscopic structure of AgNPs/rGO were studied by scanning electron microscope (SEM) (Thermo Fisher Scientific, America) operated at an accelerating voltage of 5 kV and specific surface area pore size distribution (BET) (MicrotracBEL Inc., Japan), respectively. The chemical composition analysis of GO and AgNPs/rGO prepared at 60 °C, 80 °C and 100 °C were carried out with a monochromatic Al/AgKa x-ray source operating at 15 kV and 10 mA. The Raman spectra of GO and AgNPs/rGO fabricated at 100 °C were conducted by using a LabRAM HR Evolution spectrometer (HORIBA Scientific, Japan). The effusion of silver from AgNPs/rGO-SR was determined by inductively coupled plasma emission mass spectrometer (PerkinElmer, German).

2.3. Preparation of the AgNPs/rGO

100 mg of GO was dispersed in 100 ml H_2O and adjusted the pH to 9 with sodium hydroxide, and then the mixture was sonicated for 1 h. 200 mg of $AgNO_3$ was added to a certain amount of water, and $NH_3.H_2O$ was dropped in until the solution was transparent. Then, the silver ammonia solution ($[Ag(NH_3)_2]^+$) was added to the GO solution and heated at certain temperatures in an oil bath after fully mixing. Next, sodium borohydride solution was dropped in and stirred for another 4 h. When the reaction mixture was cooled to room temperature, the AgNPs/rGO nanocomposite was obtained by vacuum filtration and washed by DI water thoroughly. The as-received AgNPs/rGO was dried in a vacuum oven at 40 °C for 10 h.

2.4. Preparation of silicon rubber (SR) membrane

The liquid rubber solution (liquid silicon rubber A: liquid silicon rubber B = 10 g: 10 g) was stirred for 10 min at room temperature, followed by degassing in a vacuum oven until the bubbles completely disappeared. Then, the mixture was coated with a coating machine and solidified for 30 min at 90 °C.

2.5. Preparation of AgNPs/rGO-SR membrane

A mixture of 10 g of liquid silicon rubber A, 10 g of liquid silicon rubber B, and 80 mg of AgNPs/rGO was stirred for 10 min, and then, the mixture had been vacuumed at room temperature until the bubbles completely disappeared. Next, the mixture was coated with a coating machine and solidified for 30 min at 90 °C.

2.6. Antibacterial activity experiments

1 ml of *E. coli* (or *S. aureus*) stored in the refrigerator at −80 °C was added to 50 ml LB medium, and was incubated to logarithmic growth with constant shaking of 120 rpm at 37 °C. The OD value of the bacterial suspension was adjusted to 1.0. A certain amount of antibacterial samples were weighed and added into 150 ml LB medium, and then added 1 ml the bacterial solution (The concentration of bacteria was 10^7 CFU ml^{-1}). The mixtures were incubated at 37 °C in an incubator shaker, and the growth of bacteria was detected by measuring the optical density at OD 600 at regular intervals. Each experiment was implemented in 2 replicates.

2.7. Antibacterial activity of AgNPs/rGO-SR and bacteriostasis bottles

SR, AgNPs/rGO-SR and bacteriostasis bottles were cut into (50 ± 2) mm × (50 ± 2) mm squares, and polyethylene terephthalate (PET) was cut into (40 ± 2) mm × (40 ± 2) mm squares, and all the samples were disinfected with 75% alcohol. Firstly, SR, AgNPs/rGO-SR and bacteriostasis bottle squares were placed into separate sterile petri dishes with the test surface uppermost. Secondly, 0.3 ml of *E. coli* or *S. aureus* (10^3 ~ 10^4 CFU ml^{-1}) was pipetted onto the samples, and PET squares were covered on the test inoculums and gently pressed down so that the test inoculum could spread to the edges. Thirdly, the petri dishes containing the inoculated samples were incubated at a temperature of (35 ± 1) °C and a relative humidity of not less than 90% for (24 ± 1) hours. Fourthly, the test specimens were put into sterile bags, and 10 ml LB cultures were added respectively, after thorough mixing, 1 ml liquid was pipetted and 10-fold serial dilutions was performed. Fifthly, 100 μl the dilutions was taken and evenly coated on the LB solid medium in the petri dishes which were incubated at 37 °C for 18 ~ 24 h. The dishes with the number of colonies containing 30 to 300 colonies were counted after incubation. Each experiment was implemented in 2 replicates.

2.8. The effusion of silver from AgNPs/rGO-SR

The effusion of silver from the AgNPs/rGO-SR was carried out as follows: 12 g of the AgNPs/rGO-SR was immersed statically in 100 ml ultrapure water at 20 °C over a period time of 7 days or at 80 °C for 2 h in dark place. The concentration of silver in soak solutions was measured by inductively coupled plasma mass spectrometer (NexlON 350×, PerkinElmer). Each experiment was implemented in 2 replicates.

3. Results and discussion

3.1. Preparation and characterization of the AgNPs/rGO

The schematic diagram of AgNPs/rGO preparation was shown in figure 1(a). GO contains polyaromatic structure and a variety of oxygen functional groups as epoxy, hydroxyl, carbonyl, and carboxyl. The epoxy groups of GO change into phenolic hydroxyl groups by ring opening reaction in alkaline condition [28]. Furthermore, the carboxyl groups ionize H^+ under alkaline conditions, making GO negatively charged, which may increase the spaces of the nanosheets by charge repulsion and be more favorable for $[Ag(NH_3)_2]^+$ intercalation and attaching to the GO nanosheets. In our experiments, $AgNO_3$ was prepared as $[Ag(NH_3)_2]^+$, and then added to GO solution. $AgNO_3$ is acidic, and the pH of GO solution will be continuous decrease if $AgNO_3$ is added. When the solution becomes acidic, GO is no longer negatively charged, and the spacing of the nanosheets may decrease, which may be difficult for Ag^+ to enter into the GO lamellar. $[Ag(NH_3)_2]^+$ is alkaline, and its addition will not decrease the pH of GO solution, nor will it reduce the GO lamellar spacing. The pH value of the GO solution was adjusted to 9 ~ 10, $[Ag(NH_3)_2]^+$ was added and mixed thoroughly. The $[Ag(NH_3)_2]^+$ might intercalate into the graphene layers and be absorbed on the nanosheets tightly, and silver iodide precipitation was hardly observed in a few minutes after adding iodide ions on the condition that the initial weight ratio of $AgNO_3$ to GO was no more than 2:1 (figure S1 is available online at stacks.iop.org/NANOX/1/010041/mmedia). The main forces between $[Ag(NH_3)_2]^+$ and GO may be π type silver ion-aromatic [24–26], and silver ion-oxygen [27] interaction, since part of the π electrons in polyaromatic structure and hydroxyl enter into the empty electron orbits of the silver ions. In addition, electrostatic interaction between carboxyl anion of GO and the $[Ag(NH_3)_2]^+$ may be another force to absorb the $[Ag(NH_3)_2]^+$ on the edges of the GO sheets. $[Ag(NH_3)_2]^+$ was reduced to AgNPs after adding $NaBH_4$ and might attach to rGO nanosheets from electron transfer. The work function of graphene (4.8 ev) was higher than that of silver (4.2 ev), thus, part of the electron of AgNPs transfered to rGO to form AgNPs/rGO heterostructures [29]. Therefore, GO could be used as a promising dispersant and carrier for AgNPs.

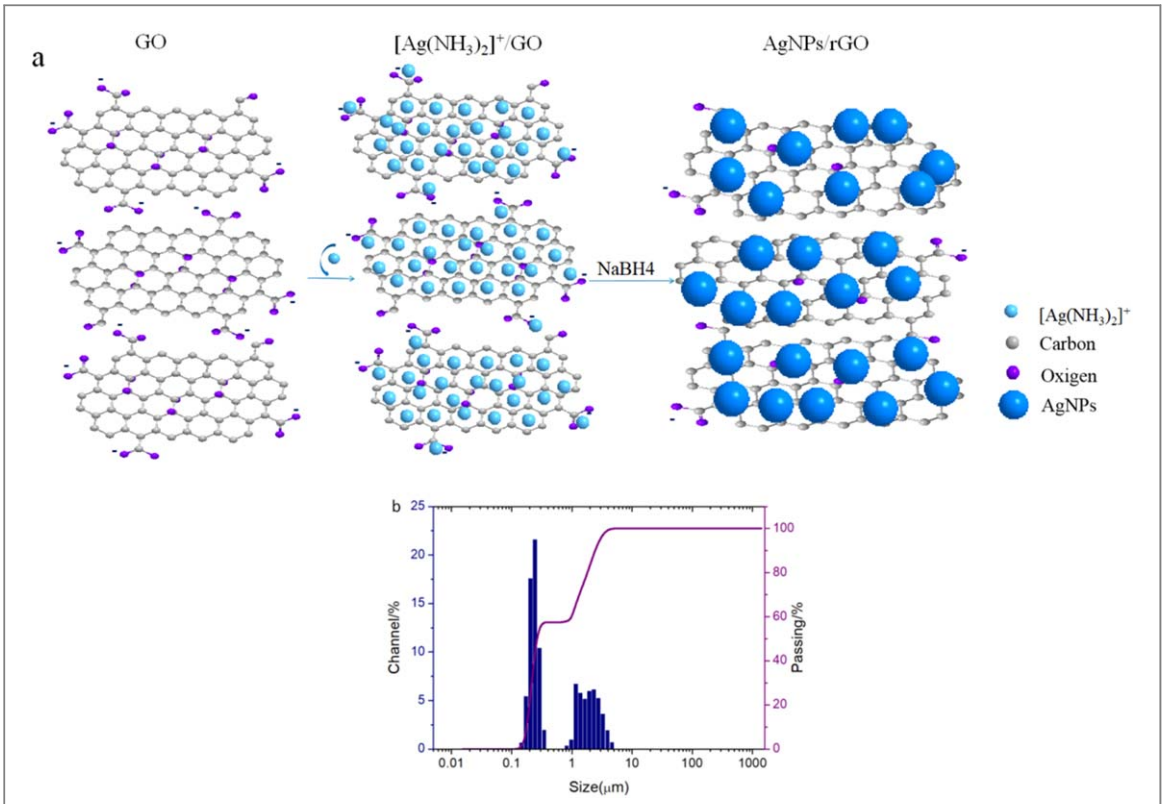

Figure 1. (a). Schematic diagram of AgNPs/rGO preparation. (b). The particle sizes distribution of GO after ultrasound in alkaline condition.

Figure 1(b) shows that GO used in our works possessed two kinds of sheets: small sheets with diameters under 400 nm and large sheets with dimensions within 5 μm, which was not completely consistent with the manufacturer's description. It is may be due to that small pieces of GO might be separated from large GO pieces during ultrasound in alkaline condition [30].

AgNPs/rGO with different mass ratios of silver nitrate and GO were synthesized and the SEM images were shown in figure 2. GO (figure 2(a)) had a laminate structure with wrinkled morphology, and as for AgNPs/rGO, there were lots of spherical AgNPs on rGO sheets (figures 2(b)–(d)). The AgNPs decorated on rGO sheets were 10–30 nm when the mass ratio of $AgNO_3$ to GO were 1:1 and 2:1. As the concentration of $AgNO_3$ increasing, more AgNPs precipitated on rGO sheets. When the mass ratio of $AgNO_3$ to GO was 4:1, the AgNPs on the rGO sheets aggregated to form large particles. Hence, AgNPs/rGO composite with small particle sizes and high AgNPs loading was obtained when the mass ratio of silver nitrate to GO was 2:1. This was not in accordance with the results of Yang groups that when the mass ratio of $AgNO_3$ to GO was more than 1:1, the sizes of AgNPs increased remarkably [20]. The reason may be that the addition of $[Ag(NH_3)_2]^+$ will not continuously reduce the pH of GO solution and decrease the spacing between GO nanosheets compared with $AgNO_3$, thus, the loaded capacity of GO on $[Ag(NH_3)_2]^+$ may be higher than that on Ag^+. Correspondingly, AgNPs/rGO with small AgNPs particle sizes and higher loading capacity can be prepared. It is reported that the size and the loading of AgNPs are the two important factors for antibacterial property [21]. AgNPs/rGO might have excellent antibacterial activity when AgNPs had small sizes and were highly loaded. The antibacterial property of AgNPs/rGO with different mass ratio of silver nitrate and GO was presented in figure S2. AgNPs/rGO with the mass ratio of 2:1 had the optimal antibacterial activity which was chosen as optimized ratio to conduct following experiments.

To investigate the real mass percentage of AgNPs, the AgNPs/rGO was calcined with muffle at 800 °C for 2 h in air. The rGO was oxidized and evaporated, while the AgNPs was reserved. The percentage of AgNPs in the AgNPs/rGO was about 67% as shown in table 1, which was much higher than that of AgNPs loading on the traditional carriers [4, 10, 11].

The characteristics of AgNPs/rGO prepared at different temperatures were investigated by XPS and BET illustrated in figure 3. Figure 3(a) demonstrates the surface composition and energy distribution of the GO and AgNPs/rGO. The binding energy peaks at 368.2 ev and 374.2 ev were corresponding to $Ag3d_{5/2}$ and $Ag3d_{3/2}$, respectively, manifesting the formation of AgNPs on rGO [16]. Further, the C1s of GO exhibited the binding energy peak at 286.9 ev, whereas the C1s binding energy peak of AgNPs/rGO was at 284.5 ev (figure 3(b)),

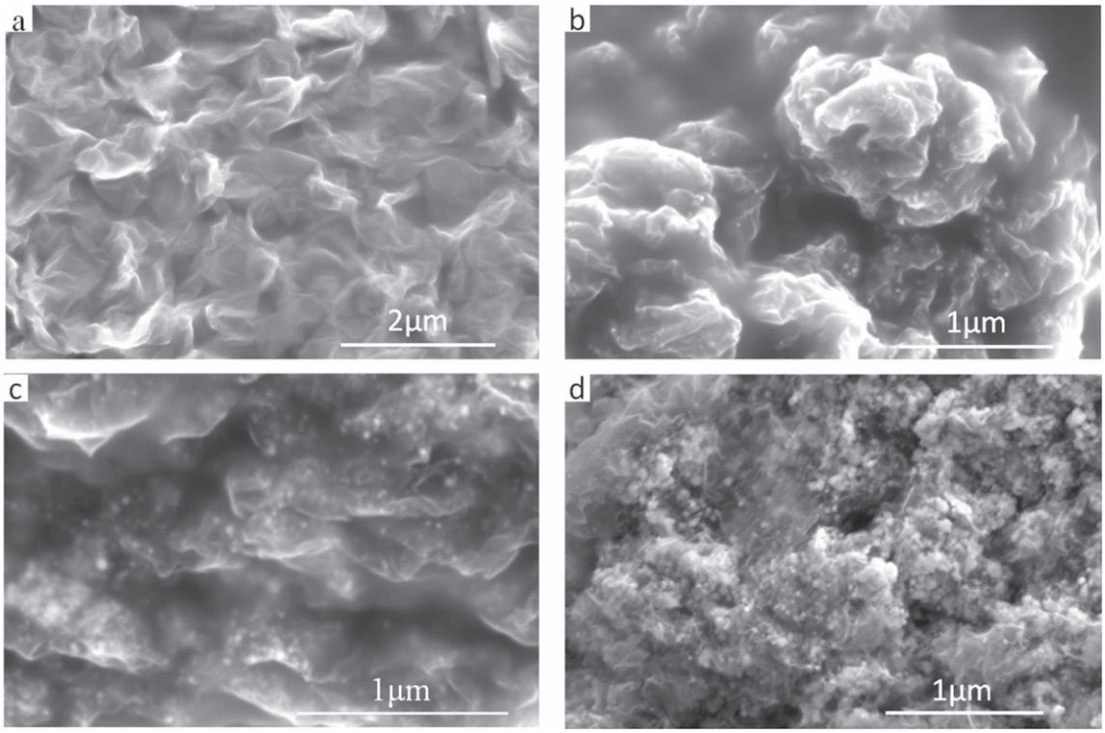

Figure 2. SEM images of (a) GO; (b)–(d) AgNPs/rGO with the initial weight ratio of $AgNO_3$ to GO being 1:1, 2:1 and 4:1, respectively.

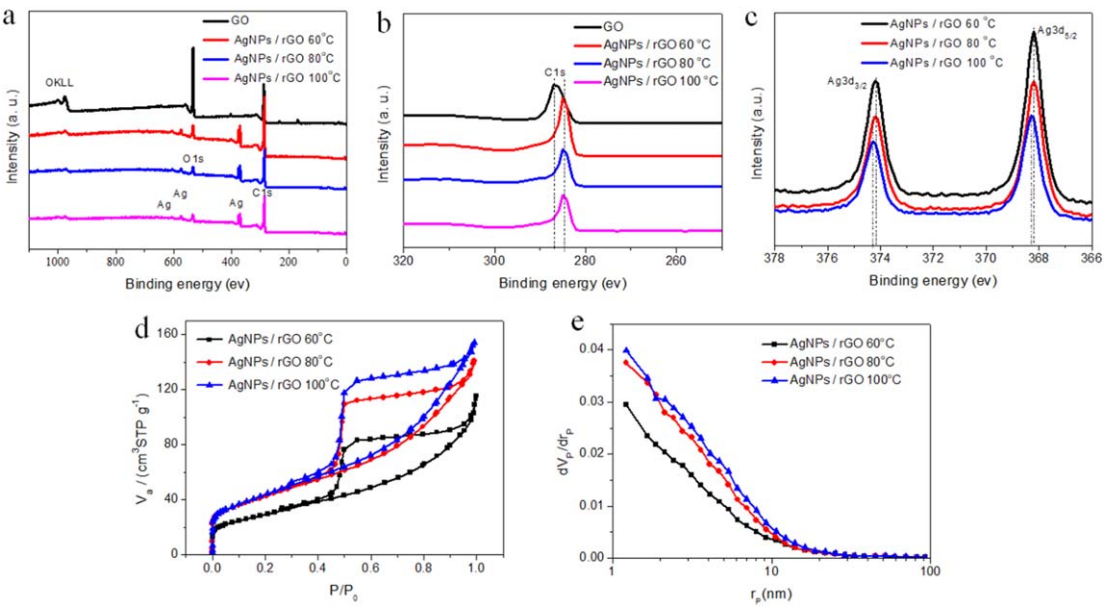

Figure 3. (a) XPS profiles of GO and AgNPs/rGO; (b) C1s profiles of GO and AgNPs/rGO; (c) XPS patterns of Ag peaks of AgNPs/rGO; (d) Adsorption and desorption curves of AgNPs/rGO prepared at 60 °C, 80 °C, 100 °C; (e) Differential pore volume distribution versus the pore radius of AgNPs/rGO prepared at 60 °C, 80 °C, 100 °C.

Table 1. The mass percentage of AgNPs in AgNPs/rGO.

Mass of AgNPs/rGO (mg)	Mass of AgNPs (mg)	Percent of AgNPs (%)
124.39 ± 0.05	84.45 ± 0.05	67.89 ± 0.10

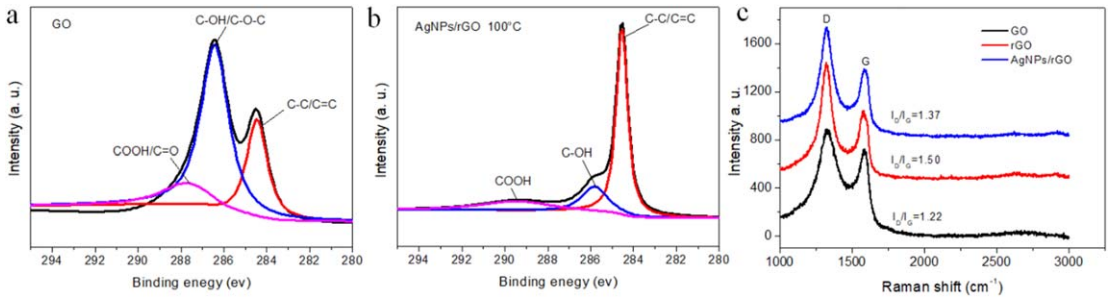

Figure 4. (a) The XPS profiles of C1s of GO; (b) XPS profiles of C1s of AgNPs/rGO prepared at 100 °C; (c) The Raman spectra of GO, rGO and AgNPs/rGO.

indicating that part of the electrons of AgNPs transfered to the aromatic carbon of rGO, which increased the shielding effect of the carbon atoms and made the nucleus less attractive to the carbon electrons [31]. The electron transfer between AgNPs and aromatic carbon of rGO allowed AgNPs attached stably to the rGO sheets. In addition, the binding energy of $Ag3d_{5/2}$ and $Ag3d_{3/2}$ of AgNPs/rGO prepared at 100 °C was higher than that of AgNPs/rGO prepared at 60 °C and 80 °C (figure 3(c)), demonstrating that electrons interaction between AgNPs and rGO of AgNPs/rGO reduced at 100 °C was stronger, that is to say, the AgNPs and rGO bound more tightly when fabricated at 100 °C.

The particle sizes of AgNPs prepared at 60 °C, 80 °C and 100 °C were compared by measuring the specific surface areas and pore diameter based on the geometric relationship between pore sizes and particle sizes. When particles are piled together, pores are bound to form between them, and the size of the pores might be proportional to that of the particles [32]. It was seen from the figure 3(d) that the adsorption-desorption curve had the characteristics of class IV adsorption lines, and the specific surface areas of AgNPs/rGO prepared at 100 °C, 80 °C and 60 °C were 126.8 $m^2\ g^{-1}$, 116.4 $m^2\ g^{-1}$ and 85.5 $m^2\ g^{-1}$, respectively. The single molecular layer adsorption ($P/P_0 < 0.1$) capacity of AgNPs/rGO prepared at 100 °C and 80 °C were higher than that of the one fabricated at 60 °C, indicating the AgNPs/rGO reduced at higher temperature possessed more micropores. Capillary condensation occurred when the relative pressure reached 0.45, indicating that lots of mesopores existed in AgNPs/rGO. The pore volumes of AgNPs/rGO fabricated at 100°C, 80 °C and 60 °C were 0.2183 $cm^3\ g^{-1}$, 0.1945 $cm^3\ g^{-1}$ and 0.1483 $cm^3\ g^{-1}$, respectively, and the number of micropores and mesopores in AgNPs/rGO fabricated at 100 °C was higher than that of the one prepared at 80 °C and 60 °C (figure 3(e)). From the above discussion, it could be speculated that AgNPs/rGO prepared at 100 °C possessed higher proportion of small sizes of AgNPs, due to the higher reaction temperature might produce more silver nanocrystalline nuclei in a short time and the AgNPs absorb on the rGO sheets with less adequate growth.

The reduction degree of oxygen-containing groups and defect information of rGO in AgNPs/rGO reduced at 100 °C was investigated by XPS and Raman spectroscopy. Figures 4(a), (b) showed the C1s XPS spectra of GO and AgNPs/rGO, respectively. The C1s peaks of C–C/C=C, C–OH/C–O–C and O–C=O/C=O of GO were observed at 284.4 eV, 286.4 eV and 287.7 eV, respectively, and the intensity of the peak of C−OH/C–O–C was higher than that of C–C/C=C, demonstrating a large number of oxygen-containing groups existed on the surface of GO nanosheets. As for C1s XPS spectra of AgNPs/rGO, the intensity of the peak of C–C/C=C increased obviously, whereas the one at 286.4 eV (C–OH) decreased sharply, which suggested that most oxygen-containing groups were reduced and part of C=C were recovered.

The Raman spectra of GO, rGO and AgNPs/rGO given in figure 4(c) exhibit two characteristic peaks, namely D- and G-band peaks at ~1324 cm^{-1} and ~1591 cm^{-1}, which demonstrate the lattice defects and edge properties, and the sp^2 state of carbon, respectively. In this work, the intensity ratios of I_D/I_G for GO, rGO and AgNPs/rGO were 1.22, 1.50, and 1.37, indicating that the defects increased when GO was reduced. It is worth noting that the I_D/I_G of AgNPs/rGO was lower than that of rGO, which might be due to AgNPs could partly repair the defects of rGO [33].

3.2. The antibacterial activity of the AgNPs/rGO

The antibacterial property of AgNPs/rGO against *S. aureus* and *E. coli* was investigated in comparison to that of GO and AgNPs. The particle sizes of AgNPs were 10 ~ 50 nm, and the diameters of AgNPs attached to rGO sheets were 10 ~ 30 nm. Some literatures reported that GO had effective antibacterial properties [14, 34], and the mechanism might be that the amphiphilic structure of GO might induce bacterial membranes to aggregate or the sharp edge of GO might cut through bacterial membranes and lead to the missing of intracellular content [35–37]. However, some paper argued that the purified GO did not have antibacterial activity [38], and GO with

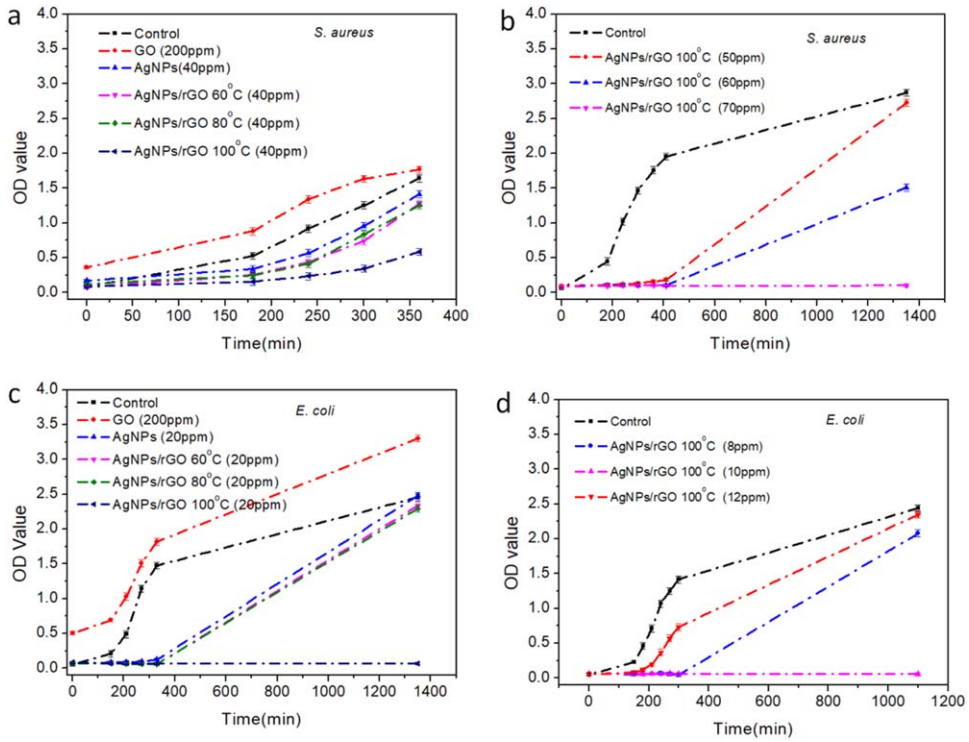

Figure 5. Bacterial growth curves of GO, AgNPs and AgNPs/rGO prepared at 60 °C, 80 °C and 100 °C against *S. aureus* and *E. coli* bacteria (a), (c). The determination of the minimum inhibitory concentration of AgNPs/rGO fabricated at 100 °C (b), (d). The concentration of GO is 200 ppm.

soluble acidic impurities showed antibacterial property [39]. In our experiments, GO hardly possessed antibacterial activity at the concentration of 200 ppm (figure 5).

It was shown from figure 5(a) that when the concentration of AgNPs and AgNPs/rGO in the culture medium was 40 ppm, the OD value of *S. aureus* kept going up as the incubation time increasing, indicating that all the samples could not completely inhibit the growth of *S. aureus*. Further, *S. aureus* with culture medium containing AgNPs/rGO fabricated at 100 °C grew more slowly, demonstrating that AgNPs/rGO prepared at 100 °C had the best antibacterial effect. Figure 5(c) showed that AgNPs and AgNPs/rGO prepared at different temperatures were effective in inhibiting the growth of *E. coli* when the incubation time was less than 300 min. However, after overnight, *E. coli* with culture medium containing AgNPs and AgNPs/rGO fabricated at 60 °C and 80 °C had grown well while the one with culture medium containing AgNPs/rGO reduced at 100 °C was completely inhibited. The results indicated that the minimum inhibitory concentration (MIC) of AgNPs/rGO prepared at 100 °C against *E. coli* was less than 20 ppm while the MIC of AgNPs with the diameters between 10 ∼ 50 nm and AgNPs/rGO fabricated at 60 °C and 80 °C against *E. coli* was more than 20 ppm. Figures 5(b), (d) showed that the MIC of AgNPs/rGO reduced at 100 °C against *S. aureus* and *E. coli* was 70 ppm and 12 ppm, respectively. It can be seen from table 2 that the MIC of AgNPs/rGO against *E. coli* in our work is lower than that of the other samples except AgNPs with triangular shape in previous studies, demonstrating that AgNPs/rGO prepared can be used as efficient antibacterial material. The AgNPs with triangular shape have better antibacterial property than the one with spherical shape, but the preparation method was complex [23, 40]. Further, the antibacterial activity of AgNPs with spherical particles was lower than that of AgNPs/rGO, suggesting that AgNPs and rGO might have synergistic antibacterial effect.

3.3. Preparation and characterization of the AgNPs/rGO-SR

Figure 6 shows the SEM images of the quick-frozen brittle sections of SR and AgNPs/rGO-Sr The SR section was composed of irregular flake aggregates with different sizes (A, B), whereas the AgNPs/rGO-SR section was evenly distributed with AgNPs and no aggregation was observed. Liquid silicone rubber molecules have a linear chain structure and prone to form flake aggregates from intermolecular and intramolecular interactions. After curing, the flake aggregates are connected by covalent bonds to form a three-dimensional network structure. rGO contains polar groups of hydroxyl and carboxyl and non-polar groups of aromatic rings. When AgNPs/rGO was added in the liquid silicon rubber, the hydroxyl and carboxyl groups in rGO might form hydrogen bonds with the oxygen [45] in -Si-O- main chains, and non-polar groups of aromatic rings might interact with

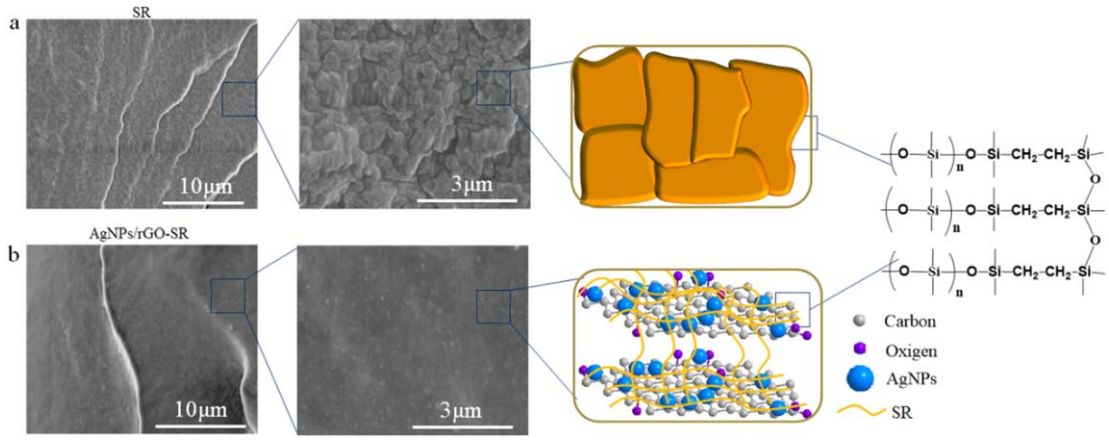

Figure 6. (a) The SEM images of frozen fractural section of SR and the proposed molecular structure based on SEM (the third); (b) The SEM images of frozen fractural section of AgNPs/rGO-SR and the proposed molecular structure based on SEM (the third).

Table 2. Comparative the antibacterial activity of AgNPs and AgNPs/rGO in our experiments and documents.

Antibacterial Samples	Diameter of AgNPs (nm)	MIC ($mg\ l^{-1}$)	Name of Bacteria	Concentration of Bacteria ($CFU\ ml^{-1}$)	Documents
AgNPs/rGO	10–30	12	*E. coli*	10^7	In this work
		70	*S. aureus*		
AgNPs/rGO	<40	12.5	*E. coli*	10^7	*Mater. Chem.*, 2011 [21]
AgNPs/rGO	11–20	100	*E. coli*	10^7	*RSC Adv.*, 2015 [22]
AgNPs/rGO	10	20	*E. coli*	10^7	*Small*, 2013 [20]
rGO/MSN/Ag	10	50	*E. coli*	10^7	*Nanotech.*, 2018 [41]
		6.25	*P.putida*		
		12.5	*Rhodococcus*		
GO-PEG-Ag	7.06 ± 2.54	2	*E. coli*	10^5	*ACS Applied Materials & Interfaces*, 2017 [38]
		5	*S. aureus*		
	7.32 ± 2.55	3	*E. coli*		
		7	*S. aureus*		
AgNPs(spherical)	39	>100	*E. coli*	10^7	*Appl. environ microb* 2007 [42]
AgNPs(triangular)	40	10			
AgNPs	4–24	>100	*E. coli*	10^7	*J Colloid Interface.* 2004 [43]
AgNPs	6.5–43.8	12.5	*Proteus vulgaris*	10^5	*Mol. Pharm.*, 2009 [44]
		12.5	*Pseudomonas aeruginosa*		
		12.5	*Salmonella abony*		

methyl and methylene [46–48]. Thus AgNPs/rGO could easily disperse in liquid silicone rubber and prevent silicone rubber molecules accumulating. The silicon rubber molecules were crosslinked in a network structure, with the AgNPs/rGO wrapped in it after curing.

3.4. The antibacterial property of the AgNPs/rGO-SR

The antibacterial property of SR, AgNPs/rGO-SR and bacteriostasis bottles against *S. aureus* and *E. coli* was measured by colony count method. The mass ratio of AgNPs/rGO to silicone rubber was 0.004 to 1, and the bacteriostasis bottles of AgNPs were commercially available. It could be seen from figure 7 that the silicon rubber had no antibacterial activity, but the AgNPs/rGO-SR and the bacteriostasis bottles had effective antibacterial property. The killing efficiency of bacteriostasis bottles against *S. aureus* and *E. coli* was 50% ± 3% and 70% ± 5% respectively, and the cell death of AgNPs/rGO-SR reached to 95% ± 3% and 98% ± 5% respectively. Encouragingly, AgNPs/rGO-SR has more effective bacteriostasis than that of the commercial

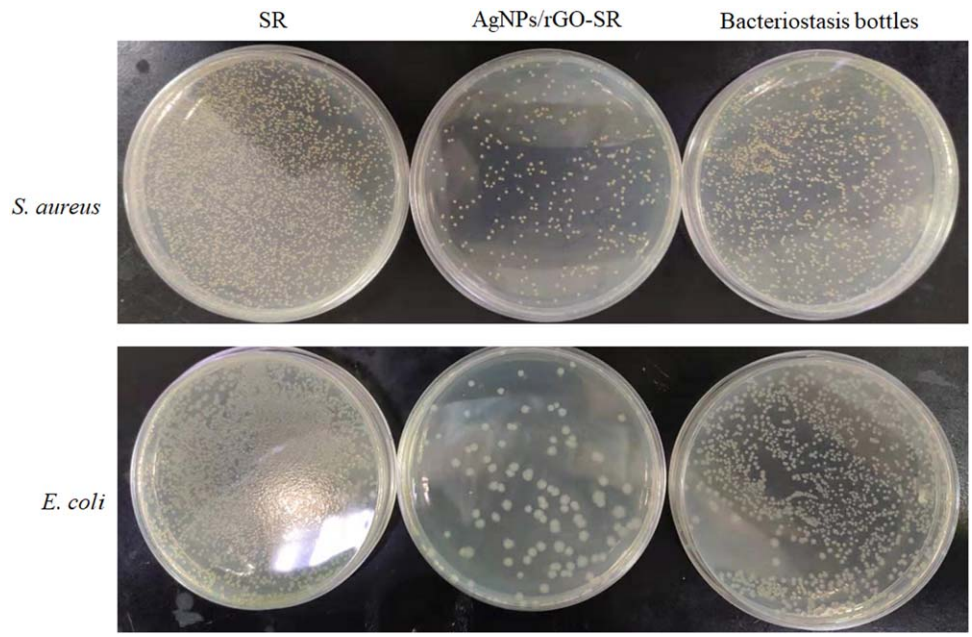

Figure 7. Images of antibacterial effect of SR, AgNPs/rGO-SR and bacteriostasis bottles.

Table 3. The effusion of silver in AgNPs/rGO-SR composite.

Effusion condition	Content of AgNPs in composite (%)	Relative standard deviation (%)	Concentration of silver in water (mg l^{-1} × 10^{-3})	Effusion percentage (%)
7d, 20 °C	0.28	56.9	1.086	0.023
2 h, 80 °C)	0.28	20.8	1.269	0.026

antibacterial milk bottles, which indicate that milk bottles might have more antibacterial efficiency if adds AgNPs/rGO to silicone rubber.

3.5. The effusion of the silver from AgNPs/rGO-SR

The effusion of silver from bacteriostatic composite not only decreases the durability, but also increases the safety hazard when the composites are used as materials of tableware, food packaging and wound dressing etc. The effusion of silver from AgNPs/rGO-SR in water was listed in table 3. The concentrations of silver in water were 1.086 × 10^{-3} mg l^{-1} and 1.269 × 10^{-3} mg l^{-1}, when AgNPs/rGO-SR was immersed in water for 7 days at 20 °C and 2 h at 80 °C, respectively, which were far less than the national standard (GB5749-2006) for drinking water that the concentration of silver must not exceed 0.05 mg l^{-1}. The effusion percentages of silver in the two soaking methods were 0.023% and 0.026%, respectively, much lower than that reported in the literatures we found: When AgNPs were added to bacterial cellulose or carbon fiber as a wound dressing or fabric, the dissolution percentage of silver exceeded 20% [3, 10, 12]. The low effusion of silver in AgNPs/rGO-SR might ensure its antibacterial durability and safety. As can be seen from the above discussion, AgNPs/rGO-SR might be used as a material for bacteriostatic bottles.

4. Conclusions

The AgNPs/rGO composite was fabricated in this study by using GO as a carrier and dispersant since GO had polyaromatic structure and oxygen-containing functional groups. AgNPs were evenly distributed on rGO sheets with particle sizes of about 10 ∼ 30 nm. The mass percent of AgNPs loading on rGO could be adjusted from 1 ∼ 67% according to the requirement of applications, whereas the synthesis of AgNPs on rGO in previous papers generally only used rGO as a carrier, and the adjustable mass percent range of AgNPs loading on rGO was much lower than that of ours [15, 16, 49]. Some of the outermost electrons of the AgNPs might enter into the delocalized electrons domains of the rGO, forming coordination bonds that enabled the AgNPs to adhere tightly to the rGO sheets. AgNPs/rGO prepared at 100 °C had the optimal bacteriostatic activity. The MIC of AgNPs/rGO fabricated at 100 °C on *E. coli* was 12 mg l^{-1} and the MIC of the one on *S. aureus* was 70 mg l^{-1}. AgNPs/

rGO could disperse evenly in the silicone rubber and the AgNPs/rGO-SR also had effective antibacterial properties. The concentration of silver effusion from the AgNPs/rGO-SR in water was about 0.001 mg l^{-1}, which was satisfied the requirement of the national standard (GB5749-2006) for drinking water. The excellent antibacterial property and low silver diffusion make AgNPs/rGO as a promising antimicrobial agent for wound dressings, bacteriostatic bottles and food packaging materials. Further, with small particle sizes and high loading capacity of AgNPs, AgNPs/rGO might have broad application prospect in the field of catalysis.

Acknowledgments

This work was supported by Beijing Municipal Science & Technology Commission No. Z181100004818004, No. Z181100001018029 and No. Z191100006119027. The authors also appreciate the technical assistance from the BGI Characterization & Quality Assurance Center and professor Luhua Lai, school of chemistry and molecular engineering, Peking University.

ORCID iDs

Di Wei https://orcid.org/0000-0002-9935-1630

References

[1] Morones J R *et al* 2005 The bactericidal effect of silver nanoparticles *Nanotechnology* **16** 2346–53
[2] Dal Lago V, França de Oliveira L, de Almeida Gonçalves K, Kobarg J and Borba Cardoso M 2011 Size-selective silver nanoparticles: future of biomedical devices with enhanced bactericidal properties *J. Mater. Chem.* **21** 12267–73
[3] OYa A and Y S 1993 Antibacterial activated carbon fiber derived from phenolic resin containing silver nitrate *Carbon* **31** 71–3
[4] Cui J *et al* 2012 Facile fabrication of carbonaceous nanospheres loaded with silver nanoparticles as antibacterial materials *J. Mater. Chem.* **22** 8121–6
[5] Chen S F *et al* 2010 Large scale photochemical synthesis of M@TiO_2 nanocomposites (M = Ag, Pd, Au, Pt) and their optical properties, CO oxidation performance, and antibacterial effect *Nano Res.* **3** 244–55
[6] Sotiriou G A, Teleki A, Camenzind A, Krumeich F, Meyer A, Panke S and Pratsinis S E 2011 Nanosilver on nanostructured silica: antibacterial activity and Ag surface area *Chem. Eng. J.* **170** 547–54
[7] Gong P *et al* 2007 Preparation and antibacterial activity of Fe_3O_4@Ag nanoparticles *Nanotechnology* **18** 285604–10
[8] Pencheva D, Bryaskova R and Kantardjiev T 2012 Polyvinyl alcohol/silver nanoparticles (PVA/AgNps) as a model for testing the biological activity of hybrid materials with included silver nanoparticles *Materials Science and Engineering:* C **32** 2048–51
[9] Liang D, Lu Z, Yang H, Gao J and Chen R 2016 Novel asymmetric wettable AgNPs/Chitosan wound dressing: *in vitro* and *in vivo* evaluation *ACS Appl. Mater. Interfaces* **8** 3958–68
[10] Maneerung T, Tokura S and Rujiravanit R 2008 Impregnation of silver nanoparticles into bacterial cellulose for antimicrobial wound dressing *Carbohydrate Polym.* **72** 43–51
[11] Yang G, Xie J, Deng Y, Bian Y and Hong F 2012 Hydrothermal synthesis of bacterial cellulose/AgNPs composite: a 'green' route for antibacterial application *Carbohydrate Polym.* **87** 2482–7
[12] Xu H, Shi X, Ma H, Lv Y, Zhang L and Mao Z 2011 The preparation and antibacterial effects of dopa-cotton/AgNPs *Appl. Surf. Sci.* **257** 6799–803
[13] Loh K P, Bao Q, Eda G and Chhowalla M 2010 Graphene oxide as a chemically tunable platform for optical applications *Nat. Chem.* **2** 1015–24
[14] Cheng C, Li S, Thomas A, Kotov N A and Haag R 2017 Functional graphene nanomaterials based architectures: biointeractions, fabrications, and emerging biological applications *Chem. Rev.* **117** 1826–914
[15] Alsharaeh E, Alazzam S, Ahmed F, Arshi N, Al-Hindawi M and Sing G K 2016 Green synthesis of silver nanoparticles and their reduced graphene oxide nanocomposites as antibacterial agents: a bio-inspired approach *Acta Metallurgica Sinica (English Letters)* **30** 45–52
[16] Alsharaeh E H and Othman A A 2014 Microwave irradiation synthesis and characterization of RGO-AgNPs/polystyrene nanocomposites *Polym. Compos.* **35** 2318–23
[17] Bai W, Nie F, Zheng J and Sheng Q 2014 Novel silver nanoparticle-manganese oxyhydroxide-graphene oxide nanocomposite prepared by modified silver mirror reaction and its application for electrochemical sensing *ACS Appl. Mater. Interfaces* **6** 5439–49
[18] Bai W, Sheng Q, Ma X and Zheng J 2015 Synthesis of silver nanoparticles based on hydrophobic interface regulation and its application of electrochemical catalysis *ACS Sustainable Chemistry & Engineering* **3** 1600–9
[19] Tang J, Chen Q, Xu L, Zhang S, Feng L, Cheng L, Xu H, Liu Z and Peng R 2013 Graphene oxide-silver nanocomposite as a highly effective antibacterial agent with species-specific mechanisms *ACS Appl. Mater. Interfaces* **5** 3867–74
[20] Zhou Y, Yang J, He T, Shi H, Cheng X and Lu Y 2013 Highly stable and dispersive silver nanoparticle-graphene composites by a simple and low-energy-consuming approach and their antimicrobial activity *Small* **9** 3445–54
[21] Xu W P *et al* 2011 Facile synthesis of silver@graphene oxide nanocomposites and their enhanced antibacterial properties *J. Mater. Chem.* **21** 4593–7
[22] Sedki M, Mohamed M B, Fawzy M, Abdelrehim D A and Abdel-Mottaleb M M S A 2015 Phytosynthesis of silver–reduced graphene oxide (Ag–RGO) nanocomposite with an enhanced antibacterial effect using Potamogeton pectinatus extract *RSC Adv.* **5** 17358–65
[23] Derakhshi M, Ashkarran A A, Bahari A and Bonakdar S 2018 Shape selective silver nanostructures decorated amine-functionalized graphene: a promising antibacterial platform *Colloids Surf.* A **545** 101–9
[24] Amma E A H G A E L 1974 Metal ion-aromatic complexes. XVIII. The preparation and molecular structure of Naphthalene-Tetrakis (si1ver perchlorate) tetrahydrate *Journal ojthe American Chemical Society* **96** 743–9
[25] Hunt G W, L T C and A A E L 1974 Metal ion-aromatic compleses XlX. Short metal-metal distances in bis (silver trifluoroacetate) benzene *Inorg. Nucl. Chem. Letters* **10** 909–13

[26] Okamoto Y, O K and K A T 1987 Capture of borane in aqueous media: role of the metal ion in the formation of aromatic 2-amino-N-heterocycle borane complexes *Polyhedron* **6** 1183–9
[27] Carrell C J, C H L, Erlebacher J and Glusker* J P 1988 Structural aspects of metal ion-carboxylate interactions *J. Am. Chem. Soc.* **110** 8651–6
[28] Chen C, Kong W, Duan H M and Zhang J 2014 Theoretical simulation of reduction mechanism of graphene oxide in sodium hydroxide solution *Phys. Chem. Chem. Phys.* **16** 12858–64
[29] Li L, Guo Y, Zhang X and Song Y 2014 Inkjet-printed highly conductive transparent patterns with water based Ag-doped graphene *J. Mater. Chem.* A **2** 19095–101
[30] Rourke J P *et al* 2011 The real graphene oxide revealed: stripping the oxidative debris from the graphene-like sheets *Angewandte Chemie* **123** 3231–35
[31] Choo D C and Kim T W 2015 Conducting transparent thin films based on silver nanowires and graphene-oxide flakes *J. Electrochem. Soc.* **162** H419–21
[32] Hu L 2017 Measurement of nano-particle size using surface area and porosity analyzer *China Powder Science and Technology* **23** 39–42
[33] Babaahmadi V, Montazer M and Gao W 2017 Low temperature welding of graphene on PET with silver nanoparticles producing higher durable electro-conductive fabric *Carbon* **118** 443–51
[34] Wierzbicki M *et al* 2019 Graphene oxide in a composite with silver nanoparticles reduces the fibroblast and endothelial cell cytotoxicity of an antibacterial nanoplatform *Nanoscale Res. Lett.* **14** 320
[35] Shaobin L *et al* 2011 Antibacterial activity of graphite, graphite oxide, graphene oxide, and reduced graphene oxide: membrane and oxidative stress *Acs Nano* **5** 6971–80
[36] Gurunathan S, Han J W, Dayem A A, Eppakayala V and Kim J H 2012 Oxidative stress-mediated antibacterial activity of graphene oxide and reduced graphene oxide in Pseudomonas aeruginosa *Int. J. Nanomedicine* **7** 5901–14
[37] Pham V T H *et al* 2015 Graphene induces formation of pores killing spherical and rod-shaped bacteria *Acs Nano* **9** 8458–67
[38] Rongtao Z *et al* 2017 Stable nanocomposite based on PEGylated and silver nanoparticles loaded graphene oxide for long-term antibacterial activity *ACS Applied Materials & Interfaces* **9** 15328–41
[39] Barbolina I, Woods C R, Lozano N, Kostarelos K, Novoselov K S and Roberts I S 2016 Purity of graphene oxide determines its antibacterial activity *2D Mater.* **3** 025025–36
[40] Li L *et al* 2017 Transparent Ag@Au–graphene patterns with conductive stability via inkjet printing *J. Mater. Chem.* C **5** 2800–6
[41] Liu R *et al* 2018 Enhanced antibacterial activity of silver-decorated sandwich-like mesoporous silica/reduced graphene oxide nanosheets through photothermal effect *Nanotechnology* **29** 105704–12
[42] Pal S, Tak Y K and Song J M 2007 Does the antibacterial activity of silver nanoparticles depend on the shape of the nanoparticle? A study of the gram-negative bacterium *Escherichia coli Appl. Environ. Microbiol.* **73** 1712–20
[43] Sondi I and Salopek-Sondi B 2004 Silver nanoparticles as antimicrobial agent: a case study on *E. coli* as a model for gram-negative bacteria *J. Colloid Interface Sci.* **275** 177–82
[44] Jaya Jain S A, Jyutika M R, Omray P, Khandelwal S and Paknikar K M 2009 Silver nanoparticles in therapeutics: development of an antimicrobial gel formulation for topical use *Mol. Pharmaceutics* **6** 1388–401
[45] Yousefi N, Lin X, Zheng Q, Shen X, Pothnis J R, Jia J, Zussman E and Kim J-K 2013 Simultaneous *in situ* reduction, self-alignment and covalent bonding in graphene oxide/epoxy composites *Carbon* **59** 406–17
[46] Cheng S, Chen X, Hsuan Y G and Li C Y 2011 Reduced graphene oxide-induced polyethylene crystallization in solution and nanocomposites *Macromolecules* **45** 993–1000
[47] Ning N, Zhang W, Yan J, Xu F, Wang T, Su H, Tang C and Fu Q 2013 Largely enhanced crystallization of semi-crystalline polymer on the surface of glass fiber by using graphene oxide as a modifier *Polymer* **54** 303–9
[48] Xu J-Z, Chen C, Wang Y, Tang H, Li Z-M and Hsiao B S 2011 Graphene nanosheets and shear flow induced crystallization in isotactic polypropylene nanocomposites *Macromolecules* **44** 2808–18
[49] Chen J, Sun L, Cheng Y, Lu Z, Shao K, Li T, Hu C and Han H 2016 Graphene oxide-silver nanocomposite: novel agricultural antifungal agent against fusarium graminearum for crop disease prevention *ACS Appl. Mater. Interfaces* **8** 24057–70